

# Assessing the Accuracy of Density Functional Approximations for Predicting Hydrolysis Reaction Kinetics

Alexander Rizzolo Epstein,<sup>†</sup> Evan Walter Clark Spotte-Smith,<sup>†</sup> Maxwell C. Venetos, Oxana Andriuc, and Kristin Aslaug Persson\*



Cite This: <https://doi.org/10.1021/acs.jctc.3c00176>



Read Online

ACCESS |



Metrics & More

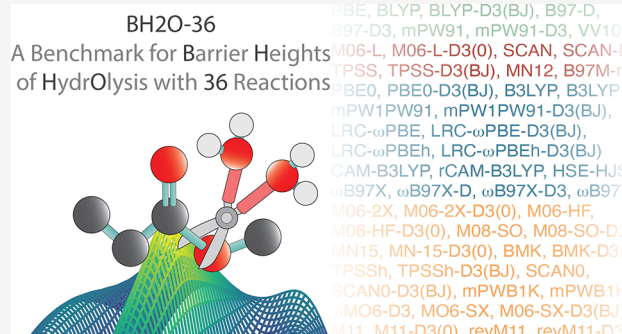


Article Recommendations



Supporting Information

**ABSTRACT:** Hydrolysis reactions are ubiquitous in biological, environmental, and industrial chemistry. Density functional theory (DFT) is commonly employed to study the kinetics and reaction mechanisms of hydrolysis processes. Here, we present a new data set, Barrier Heights for HydrOlysis - 36 (BH2O-36), to enable the design of density functional approximations (DFAs) and the rational selection of DFAs for applications in aqueous chemistry. BH2O-36 consists of 36 diverse organic and inorganic forward and reverse hydrolysis reactions with reference energy barriers  $\Delta E^\ddagger$  calculated at the CCSD(T)/CBS level. Using BH2O-36, we evaluate 63 DFAs. In terms of mean absolute error (MAE) and mean relative absolute error (MRAE),  $\omega$ B97M-V is the best-performing DFA tested, while MN12-L-D3(BJ) is the best-performing pure (nonhybrid) DFA. Broadly, we find that range-separated hybrid DFAs are necessary to approach chemical accuracy (0.043 eV). Although the best-performing DFAs include a dispersion correction to account for long-range interactions, we find that dispersion corrections do not generally improve MAE or MRAE for this data set.



## INTRODUCTION

Hydrolysis reactions are among the most important and widely studied reaction classes in chemistry. In addition to its relevance in biological and environmental processes,<sup>1–5</sup> hydrolysis finds myriad technical applications, including in pharmaceuticals,<sup>6–8</sup> total organic synthesis, waste treatment,<sup>9</sup> and the deconstruction of polymers.<sup>10,11</sup> Due to the ubiquity and technological importance of hydrolysis, many experimental and theoretical studies have been undertaken to understand the fundamental reaction mechanism involved, including the elementary reaction steps, reaction energy barriers (from which rate coefficients can be calculated), and the effect of solvent molecules.<sup>12–20</sup>

First-principles quantum chemical calculations are a powerful tool for the prediction and analysis of reaction mechanisms. This frequently involves performing calculations to predict the geometries and subsequently the energies of reactants, products, intermediates, and transition states (TSs) along the reaction pathway. In particular, density functional theory (DFT) is widely used for studies of small-molecule hydrolysis<sup>21–46</sup> due to its reasonably high accuracy and low cost compared to more advanced wave function methods. A particularly popular choice of density functional approximation (DFA) in such studies is B3LYP.<sup>21–38</sup> Beyond DFT, common methods employed in computational studies of hydrolysis reactions include Hartree–Fock (HF)<sup>23,25,31,35,45</sup> and second-order Møller–Plesset perturbation theory

(MP2),<sup>23–25,30,32,47,48</sup> with less frequent use of higher-order Møller–Plesset perturbation theory,<sup>24,30,49</sup> coupled-cluster,<sup>25,47</sup> and configuration-interaction methods.<sup>30,31,48</sup>

While numerous benchmark studies have been conducted to evaluate the performance of various exchange–correlation DFAs for the prediction of reaction thermochemistry,<sup>50–58</sup> there exist relatively few such benchmark studies focused on reaction kinetics,<sup>59–65</sup> and even fewer include hydrolysis reactions. In one study of hydrolysis, Ribeiro et al.<sup>66</sup> assessed the performance of 52 DFAs, Hartree–Fock, and 4 post-Hartree–Fock methods (MP2, MP3, MP4, and CCSD) against the coupled-cluster singles, doubles, and quasiperturbative triplets wave function method extrapolated to the complete basis set limit (CCSD(T)/CBS) in predicting the reaction and activation energies involved in the hydrolysis of dimethylphosphate as a model system for phosphodiester bonds. They performed calculations both in vacuum and with an implicit solvent and identified the same two global hybrid meta-generalized gradient approximation (hybrid meta-GGA) DFAs (MPWB1K and MPW1B95) to have the lowest mean

Received: February 13, 2023

Table 1. Exchange–Correlation DFAs Considered in This Benchmark Study<sup>a</sup>

Name	Type	Hybrid Type	HF Exchange	Dispersion Correction	References
PBE	GGA	N/A	N/A	None	68
PBE-D3(BJ)	GGA	N/A	N/A	D3(BJ)	68, 69
BLYP	GGA	N/A	N/A	None	70, 71
BLYP-D3(BJ)	GGA	N/A	N/A	D3(BJ)	69–71
B97-D	GGA	N/A	N/A	D2	72
B97-D3	GGA	N/A	N/A	D3(0)	69, 72
mPW91	GGA	N/A	N/A	None	73
mPW91-D3(BJ)	GGA	N/A	N/A	D3(BJ)	69, 73
VV10	GGA	N/A	N/A	VV10	74
rVV10	GGA	N/A	N/A	rVV10	75
M06-L	meta-GGA	N/A	N/A	None	76
M06-L-D3(0)	meta-GGA	N/A	N/A	D3(0)	76, 77
SCAN	meta-GGA	N/A	N/A	None	78
SCAN-D3(BJ)	meta-GGA	N/A	N/A	D3(BJ)	69, 78
TPSS	meta-GGA	N/A	N/A	None	79
TPSS-D3(BJ)	meta-GGA	N/A	N/A	D3(BJ)	69, 79
MN12-L	meta-GGA	N/A	N/A	None	80
MN12-L-D3(BJ)	meta-GGA	N/A	N/A	D3(BJ)	69, 80
B97M-rV	meta-GGA	N/A	N/A	rVV10	75, 81
PBE0	hybrid GGA	global	0.25	None	82, 83
PBE0-D3(BJ)	hybrid GGA	global	0.25	D3(BJ)	69, 82, 83
B3LYP	hybrid GGA	global	0.20	None	70, 71, 84
B3LYP-D3(BJ)	hybrid GGA	global	0.20	D3(BJ)	69–71, 84
mPW1PW91	hybrid GGA	global	0.25	None	73
mPW1PW91-D3(BJ)	hybrid GGA	global	0.25	D3(BJ)	69, 73
LRC- $\omega$ PBE	hybrid GGA	range-separated	0.0; 1.0	None	85
LRC- $\omega$ PBE-D3(BJ)	hybrid GGA	range-separated	0.0; 1.0	D3(BJ)	69, 85
LRC- $\omega$ PBEh	hybrid GGA	range-separated	0.2; 1.0	None	86
LRC- $\omega$ PBEh-D3(BJ)	hybrid GGA	range-separated	0.2; 1.0	D3(BJ)	69, 86
CAM-B3LYP	hybrid GGA	range-separated	0.19; 0.65	None	87
CAM-B3LYP-D3(0)	hybrid GGA	range-separated	0.19; 0.65	D3(BJ)	77, 87
rCAM-B3LYP	hybrid GGA	range-separated	0.18; 0.65	None	88
rCAM-B3LYP-D3(0)	hybrid GGA	range-separated	0.18; 1.13	D3(BJ)	77, 88
HSE-HJS	hybrid GGA	range-separated	0.25; 0.0	None	89, 90
HSE-HJS-D3(BJ)	hybrid GGA	range-separated	0.25; 0.0	D3(BJ)	69, 89, 90
$\omega$ B97X	hybrid GGA	range-separated	0.16; 1.0	None	91
$\omega$ B97X-D	hybrid GGA	range-separated	0.22; 1.0	D2	72, 92
$\omega$ B97X-D3	hybrid GGA	range-separated	0.20; 1.0	D3(0)	77, 93
$\omega$ B97X-V	hybrid GGA	range-separated	0.17; 1.0	VV10	74, 94
M06-2X	hybrid meta-GGA	global	0.54	None	95
M06-2X-D3(0)	hybrid meta-GGA	global	0.54	D3(0)	77, 95
M06-HF	hybrid meta-GGA	global	1.0	None	95
M06-HF-D3(0)	hybrid meta-GGA	global	1.0	D3(0)	77, 95
M08-SO	hybrid meta-GGA	global	0.57	None	96
M08-SO-D3(0)	hybrid meta-GGA	global	0.57	D3(0)	77, 96
MN15	hybrid meta-GGA	global	0.44	None	97
MN15-D3(0)	hybrid meta-GGA	global	0.44	D3(0)	77, 97
BMK	hybrid meta-GGA	global	0.42	None	98
BMK-D3(BJ)	hybrid meta-GGA	global	0.42	D3(BJ)	69, 98
TPSSh	hybrid meta-GGA	global	0.1	None	99
TPSSh-D3(BJ)	hybrid meta-GGA	global	0.1	D3(BJ)	69, 99
SCAN0	hybrid meta-GGA	global	0.25	None	100
SCAN0-D3(BJ)	hybrid meta-GGA	global	0.25	D3(BJ)	69, 100
mPWB1K	hybrid meta-GGA	global	0.44	None	101
mPWB1K-D3(BJ)	hybrid meta-GGA	global	0.44	D3(BJ)	69, 101
$\omega$ M06-D3	hybrid meta-GGA	range-separated	0.27; 1.0	D3(0)	77, 93
M06-SX	hybrid meta-GGA	range-separated	0.34; 1.0	None	102

Table 1. continued

Name	Type	Hybrid Type	HF Exchange	Dispersion Correction	References
M06-SX-D3(BJ)	hybrid meta-GGA	range-separated	0.34; 1.0	D3(0)	69, 102
M11	hybrid meta-GGA	range-separated	0.43; 1.0	None	103
M11-D3(0)	hybrid meta-GGA	range-separated	0.43; 1.0	D3(0)	77, 103
revM11	hybrid meta-GGA	range-separated	0.23; 1.0	None	104
revM11-D3(0)	hybrid meta-GGA	range-separated	0.23; 1.0	D3(0)	77, 104
$\omega$ B97M-V	hybrid meta-GGA	range-separated	0.15; 1.0	VV10	74, 105

<sup>a</sup>For range-separated hybrid DFAs, the short-range and long-range fractions of HF exact exchange are provided, separated by a semicolon.

absolute error (MAE) values (<1 kcal/mol) both overall and with respect to activation energies exclusively. In addition, Pereira et al.<sup>67</sup> benchmarked 40 DFAs, as well as the self-consistent-charge density-functional tight-binding method (SCC-DFTB) and 4 semiempirical methods (AM1, PM3, PM6, and PDDG) against CCSD(T)/CBS//MP2/aug-cc-pVTZ in the study of the hydrolysis of glycosidic bonds. Using a 22-atom model system, they compared the performance of the methods under investigation both in geometry optimizations (bond lengths and angles) and electronic energy calculations (barrier heights and reaction energies). Their findings show that the inclusion of HF exchange generally correlates with an increase in accuracy, whereas the effect of adding semiempirical D3 dispersion corrections on the accuracy of barrier heights can be either positive or negative. While these studies are significant contributions to the use of DFAs for studying hydrolysis, the class of reagents that can undergo hydrolysis reactions is extensive, and thus, additional work is needed to assess the performance of DFAs for a broader range of hydrolysis applications.

Here we present a set of 36 forward and reverse hydrolysis reactions that we call BH2O-36 (Barrier Heights of HydrOlysis - 36). The reactions in BH2O-36 are diverse, including single-step  $S_N2$  and multistep addition–elimination mechanisms; water-assisted and nonwater-assisted reactions; acidic and basic hydrolysis; as well as a range of functional groups. We use BH2O-36 to benchmark the performance of 63 DFT methods in four different classes: the generalized gradient approximation (GGA), meta-generalized gradient approximation (meta-GGA), hybrid GGA, and hybrid meta-GGA levels of theory. We assess the ability of DFAs to predict the electronic energy barriers of hydrolysis reactions at fixed geometries, referencing to energy values calculated using CCSD(T)/CBS. We also consider predictions of hydrolysis reaction energies. Based on these results, we make specific recommendations of DFAs for use in studying hydrolysis kinetics and general observations regarding particular types of DFAs or features included in DFA design.

## COMPUTATIONAL METHODS

The 63 exchange–correlation DFAs considered in this study are listed in Table 1. Selection of DFAs was essentially arbitrary but based on a number of practical factors, including diversity in terms of DFA type (GGA, meta-GGA, hybrid, etc.), DFA family (e.g., Perdew nonempirical DFAs or Minnesota DFAs), and previous performance in benchmark studies of reaction thermochemistry and energy barriers.<sup>65,106</sup> Of these 63 DFAs, 10 are GGA, 9 are meta-GGA, 20 are hybrid GGA, and 24 are hybrid meta-GGA. For hybrid DFAs, Table 1 lists whether the DFA is a global hybrid, which applies a fraction of Hartree–Fock (HF) exact electronic exchange

energy uniformly through space, or a range-separated hybrid, which has HF contributions that vary spatially. Range-separated hybrids include different fractions of HF exchange at long-range and short-range and use a splitting function, commonly involving the error function, to interpolate between those two fractions. By spatially varying the fraction of HF exchange, range-separated hybrids aim to improve upon global hybrids to further reduce the detrimental self-interaction error inherent to DFAs and to improve the treatment of long-range electron–electron interactions.<sup>91</sup> DFAs were evaluated both with and without dispersion corrections unless they were designed specifically with an included dispersion correction. The dispersion correction chosen for most DFAs was the empirical D3 dispersion correction, either with the original (D3(0))<sup>77</sup> or the Becke–Johnson (D3(BJ))<sup>69</sup> damping functions. The difference between D3(0) and D3(BJ) is typically small, and so the choice of D3 correction should not be significant;<sup>69</sup> that said, in general, the D3 correction more commonly used in the literature and in previous benchmark studies was chosen. Some DFAs alternatively employ the D2 dispersion correction,<sup>72</sup> such as B97-D<sup>72</sup> and  $\omega$ B97X-D,<sup>92</sup> or the VV10<sup>74</sup> and rVV10<sup>75</sup> nonlocal correlation DFAs, such as VV10,<sup>74</sup> B97M-rV,<sup>81</sup> and  $\omega$ B97M-V.<sup>105</sup> The notation D3(0) or D3(BJ) is used here for a dispersion correction appended during the calculation, while all other notation indicates the DFA was designed with the dispersion correction. In the Supporting Information, we consider the effect of the more recently developed DFT-D4 semiempirical dispersion correction on a small subset of DFAs (Tables S5).<sup>107</sup> DFT-D4 is not included in the Q-Chem major version that was used for all other data in this study (version 5), so we instead used Q-Chem version 6.0.2. Because Q-Chem version 6 has significant changes over version 5, we caution against placing significant weight on any comparisons between DFT-D4-corrected and other DFAs.

All calculations apart from the DFT-D4 study were performed using Q-Chem versions 5.3.2 and 5.4.2.<sup>108</sup> We performed all calculations using a tight threshold for the neglect of two-electron integrals ( $10^{-14}$ ) to improve calculation precision and convergence, and we used the standard integration grid SG-3<sup>109</sup> for all atoms. Unless otherwise stated, all optimization calculations to ground-state potential-energy surface minima (reactants and products) and TSs were conducted using the split-valence def2-SVPD basis set,<sup>110</sup> and all final energy calculations using DFT were performed with the larger triple- $\zeta$  def2-TZVPPD basis set. In a previous benchmark study from Mardirossian and Head-Gordon,<sup>106</sup> it was found that def2-TZVPPD had nearly the same accuracy as the quadruple- $\zeta$  def2-QZVPPD basis set, making it appropriate for benchmark studies. We note that some TSs were optimized using initial guess structures taken from the literature; where

Table 2. Reactions Included in the BH2O-36 Benchmark Set<sup>4a</sup>

Number	Reaction	Class	Conditions	Assisted	Refs.
1		Anhydride	Acid/Base	No	N/A
2		Amide	Base	Yes	23
3		Amide	Base	Yes	23
4		Borohydride	Neutral/Acid	No	115
5		Carbonate	Base	No	116
6		Diazonium	Acid	No	26
7		Epoxide	Acid	No	117
8		Epoxide	Acid	No	117
9		Epoxide	Base	No	N/A
10		Epoxide	Base	No	N/A
11		Ester	Base	No	N/A
12		Furan	Acid	Yes	41
13		Furan	Acid	Yes	41
14		Furan	Acid	Yes	41
15		Imine	Base	No	48
16		Iminium	Acid	No	48
17		Lactone	Base	No	30
18		Phosgene	Acid/Base	No	118

<sup>4a</sup>For reactions where initial transition-state structures were taken from the literature, the reference indicates the source of the structure.<sup>23,25,26,30,41,48,115–118</sup>

literature structures were not available, we conducted TS searches by hand. In evaluating the performance of DFAs for calculating electronic energy, we perform single-point energy evaluations in vacuum.

All TSs were initially optimized in vacuum using the strongly constrained and appropriately normed (SCAN) meta-GGA DFA (Table S1).<sup>78</sup> Reaction end points were then optimized by perturbing the TS along the reaction coordinate in both

**Table 3.** Mean Absolute Errors (MAEs) and Mean Relative Absolute Errors (MRAEs) of 63 Exchange–Correlation DFAs on the BH2O-36 Benchmark Set, Referenced to CCSD(T)/CBS Energies Calculated from SCAN-Optimized Geometries<sup>a</sup>

Name	MAE (eV)	Rank	MRAE	Rank	Name	MAE (eV)	Rank	MRAE	Rank
$\omega$ B97M-V	0.030	1	0.078	1	M06-2X	0.077	29	0.277	38
CAM-B3LYP-D3(0)	0.044	2	0.090	2	SCAN	0.109	44	0.204	26
M06-SX-D3(BJ)	0.049	6	0.104	4	B3LYP-D3(BJ)	0.082	32	0.305	41
$\omega$ M06-D3	0.045	3	0.111	8	mPW1PW91-D3(BJ)	0.087	37	0.274	36
$\omega$ B97X-D3	0.049	7	0.109	6	rCAM-B3LYP	0.088	38	0.267	35
$\omega$ B97X-V	0.047	4	0.128	13	SCAN-D3(BJ)	0.111	45	0.219	30
MN15	0.055	12	0.109	5	B3LYP	0.084	36	0.380	47
BMK-D3(BJ)	0.057	14	0.100	3	TPSSH-D3(BJ)	0.117	49	0.260	34
$\omega$ B97X-D	0.050	8	0.124	11	rCAM-B3LYP-D3(0)	0.088	39	0.378	46
CAM-B3LYP	0.047	5	0.140	15	revM11	0.102	42	0.367	44
M11	0.052	10	0.123	10	TPSSH	0.111	47	0.303	40
BMK	0.063	19	0.110	7	LRC- $\omega$ PBEh-D3(BJ)	0.102	41	0.382	48
mPW1PW91	0.063	18	0.113	9	SCAN0-D3(BJ)	0.099	40	0.401	50
M08-SO	0.053	11	0.142	17	revM11-D3(0)	0.104	43	0.472	53
$\omega$ B97X	0.056	13	0.143	18	PBE	0.166	55	0.377	45
HSE-HJS	0.071	25	0.128	12	PBE-D3(BJ)	0.171	57	0.338	43
M06-SX	0.051	9	0.215	29	M06-L	0.111	46	0.490	55
PBE0	0.073	26	0.136	14	mPW91-D3(BJ)	0.180	59	0.315	42
M08-SO–D3(0)	0.065	20	0.163	21	M06-L-D3(0)	0.111	48	0.493	56
MN12-L-D3(BJ)	0.067	21	0.182	22	B97-D	0.155	52	0.488	54
HSE-HJS-D3(BJ)	0.071	24	0.157	19	TPSS	0.166	54	0.449	52
M11-D3(0)	0.058	15	0.225	31	mPW91	0.168	56	0.432	51
MN12-L	0.067	22	0.186	24	TPSS-D3(BJ)	0.172	58	0.401	49
mPWB1K	0.082	31	0.141	16	B97-D3	0.155	53	0.498	57
MN15-D3(0)	0.062	17	0.230	32	M06-HF-D3(0)	0.152	50	0.770	62
SCAN0	0.069	23	0.204	27	M06-HF	0.152	51	0.772	63
PBE0-D3(BJ)	0.074	27	0.183	23	rVV10	0.183	60	0.550	59
mPWB1K-D3(BJ)	0.079	30	0.159	20	VV10	0.183	61	0.540	58
B97M-rV	0.060	16	0.302	39	BLYP	0.187	62	0.711	61
LRC- $\omega$ PBEh	0.083	35	0.200	25	BLYP-D3(BJ)	0.190	63	0.623	60
LRC- $\omega$ PBE	0.082	34	0.206	28					
M06-2X-D3(0)	0.076	28	0.275	37					
LRC- $\omega$ PBE-D3(BJ)	0.082	33	0.247	33					

<sup>a</sup>DFAs are listed in order of their average rankings in terms of MAE and MRAE for barrier heights calculated in vacuum.

directions. To assess the influence of the DFA used for the optimization, we considered the effects of optimizing geometries with  $\omega$ B97M-V, but the variation in the ranking of DFAs was insignificant (Figure S2 and Table S3).

Reference energies approximate the CCSD(T)/CBS level of theory. In order to avoid computationally demanding CCSD(T) calculations at large basis sets, HF exchange and MP2 correlation energy were first calculated with the def2-TZVPP ( $\zeta_1 = 3$ ) and def2-QZVPP ( $\zeta_2 = 4$ ) basis sets. These values were then extrapolated to the CBS limit using a scheme similar to the Weizmann-1 extrapolation:<sup>111,112</sup>

$$E_{\text{CBS}}^{\text{HF}} \approx E_{\zeta_2} + \frac{E_{\zeta_2} - E_{\zeta_1}}{\exp(\alpha(\sqrt{\zeta_2} - \sqrt{\zeta_1})) - 1} \quad (1)$$

$$E_{\text{CBS}}^{\text{MP2}} \approx \frac{\zeta_1^\beta E_{\zeta_1} - \zeta_2^\beta E_{\zeta_2}}{\zeta_1^\beta - \zeta_2^\beta} \quad (2)$$

with  $\alpha = 7.880$ ,  $\beta = 2.970$  as previously calculated for the chosen basis sets by Neese and Valeev.<sup>113</sup> Then, to calculate CCSD(T)/CBS energy, the difference between CCSD(T) and MP2 using the def2-TZVP basis set was calculated,<sup>114</sup> yielding

$$E_{\text{CBS}}^{\text{CCSD(T)}} = E_{\text{CBS}}^{\text{HF}} + E_{\text{CBS}}^{\text{MP2}} + (E_{\text{def2-TZVP}}^{\text{CCSD(T)}} - E_{\text{def2-TZVP}}^{\text{MP2}}) \quad (3)$$

This method is based on the notion that the difference between MP2 and CCSD(T) energies should be roughly the same regardless of basis set size. To ensure that this method provides reliable reference energy barriers, reaction barriers for a smaller set of 24 reactions from BH2O-36 were calculated with HF and CCSD extrapolated to the CBS limit using def2-TZVPP and def2-QZVPP as above, and the (T) term extrapolated to the CBS limit using the def2-SVP and def2-TZVP basis sets with  $\alpha = 10.390$ ,  $\beta = 2.400$ . The MAE for the method using eq 3 with respect to the direct extrapolation of CCSD(T) was 0.016 eV, which is well within “chemical accuracy” of 0.043 eV.

In this study, average errors compared to reference data are reported in two ways. For each DFA  $f$  considered, the MAE is calculated as

$$\text{MAE} = \frac{1}{n} \sum_r^R |V_{f,r} - V_{\text{reference},r}| \quad (4)$$

where  $n$  is the number of reactions, and the sum is over the set of reactions  $R$ . Reaction barriers can vary significantly in magnitude, and as a result, the MAE may overemphasize reactions with larger energy barriers, where large errors may be more likely. Because of this, the mean relative absolute error (MRAE) is also calculated as

$$\text{MRAE} = \frac{1}{n} \sum_r \frac{|V_f - V_{\text{reference}}|}{V_{\text{reference}}} \quad (5)$$

For completeness, we have also analyzed the mean signed error (MSE) of the DFAs on the benchmark set (Figure S1 and Table S2). The MSE can provide valuable information about the tendency of a DFA to over- or underestimate barriers, but because it can be misleading when considering the overall accuracy of a method, we do not use it as a metric to rank the performance of DFAs for hydrolysis reactions.

**BH2O-36 Data Set.** The reactions included in BH2O-36 are listed in Table 2. Where possible, we took the geometries for our initial guesses from the literature. For each reaction listed, both the forward and reverse reaction were considered. BH2O-36 contains 36 total reactions representing 12 unique classes of hydrolysis reactions (anhydride, amide, borohydride, carbonate, diazonium, epoxide, ester, furan, imine, iminium, lactone, and phosgene/chlorinated hydrocarbon). The data set is evenly split between acidic (16) and basic (16) hydrolysis reactions, with a small number of reactions that can occur in any aqueous environment (4). While most reaction mechanisms included in BH2O-36 do not include more than one explicit water molecule, the amide (2 and 3) and furan (12–14) reactions are water-assisted.

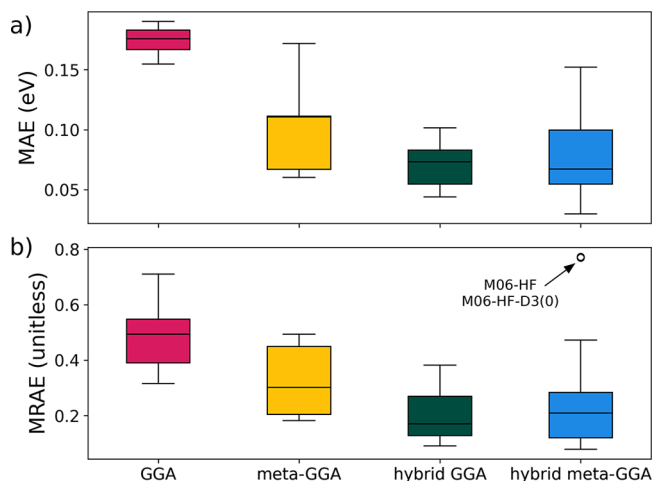
## RESULTS AND DISCUSSION

Table 3 lists the MAE, MRAE, and associated rankings of the 63 DFAs in Table 1 for barrier heights calculated in vacuum. DFAs are listed in order based on the average of the two rankings. This is meant to reduce bias toward any one particular metric. However, we note that rankings between metrics are qualitatively similar. The top two DFAs ( $\omega$ B97M-V and CAM-B3LYP-D3(0)) are identical across both metrics, and only 7 DFAs appear in the bottom 5 of either ranking. As such, either MAE or MRAE could be reasonably used to draw conclusions on the DFAs considered.

With an MAE of 0.030 eV and an MRAE of 0.078, the range-separated hybrid meta-GGA DFA  $\omega$ B97M-V is the best-suited DFA tested for calculations of hydrolysis energy barriers within the BH2O-36 benchmark set.  $\omega$ B97M-V ranks first in both metrics studied, and it outperforms by considerable margins: the MAE of  $\omega$ B97M-V is 31.8% lower than the second-ranked DFA (CAM-B3LYP-D3(0)), and the MRAE is 15.3% lower than the second-ranked DFA (also CAM-B3LYP-D3(0)). Beyond  $\omega$ B97M-V, the differences between DFAs are less pronounced, and exact rankings are perhaps less meaningful. Other well-performing DFAs include the dispersion-corrected range-separated hybrid GGA DFAs based on B97<sup>119</sup> ( $\omega$ B97X-V,<sup>94</sup>  $\omega$ B97X-D3,<sup>93</sup> and  $\omega$ B97X-D<sup>92</sup>), the range-separated hybrid GGA DFAs CAM-B3LYP-D3(0) and CAM-B3LYP,<sup>87</sup> and several DFAs derived from Minnesota DFAs—namely, the range-separated meta-GGA hybrids M06-SX-D3(BJ)<sup>102</sup> and  $\omega$ M06-D3<sup>93</sup> as well as the global meta-GGA hybrid MN15.<sup>97</sup> These DFAs are all designed for general-purpose use with main-group elements (and, in some cases, transition metals) and have previously performed well in broad benchmarks of reaction thermochemistry and barrier heights.<sup>106</sup> The BMK DFA,<sup>98</sup> which was designed specifically for calculations involving kinetics, achieves an MRAE value of only 0.100 when modified with the D3(BJ) dispersion correction. It also bears mention that the commonly used DFA B3LYP is among the poorest performing DFAs, ranking

36th in terms of MAE and 47th in terms of MRAE. The dispersion-corrected DFA B3LYP-D3(BJ) performs somewhat better (32nd in terms of MAE, 41st in terms of MRAE) but is still lacking compared to many other DFAs that have been highlighted here.

Figure 1 shows the accuracy of the four families of DFAs considered here—GGA, meta-GGA, hybrid GGA, and hybrid



**Figure 1.** Performance of different families of exchange–correlation DFAs (GGA, meta-GGA, hybrid GGA, and hybrid meta-GGA) in calculating hydrolysis energy barriers from fixed SCAN-optimized geometries in terms of MAE (a) and MRAE (b) in vacuum. The median is represented by a black bar within the box defined by the upper and lower quartiles of the data. Outliers are indicated by empty circles and emphasized with arrows. Extreme values (not including outliers) are indicated by the bars above and below the boxes.

meta-GGA. At a high level, we observe that local GGA DFAs systematically underperform in calculating hydrolysis reaction energy barriers. On average, the GGA DFAs considered here have an MAE of 0.174 eV and an MRAE of 0.487. As a result, we would not generally recommend the use of GGA DFAs for applications in hydrolysis kinetics. The addition of second-derivative terms to meta-GGA DFAs leads to a significant improvement overall, though notably, the best-performing GGA DFAs tend to outperform the worst-performing meta-GGA DFAs (depending on the metric, TPSS-D3(BJ)<sup>79</sup> or M06-L-D3(0)<sup>76</sup>). Several meta-GGA DFAs, especially MN12-L,<sup>80</sup> MN12-L-D3(BJ), and B97M-rV,<sup>81</sup> achieve low MAE values ( $\sim$ 0.06 eV) and should be considered, especially where computational resources are constrained.

The addition of Hartree–Fock exact exchange in hybrid DFAs also leads to a general improvement over pure DFAs. Interestingly, in spite of the dominant performance of  $\omega$ B97M-V, the hybrid meta-GGA DFAs exhibit higher error on average than the hybrid GGA DFAs, which is somewhat unexpected due to the greater complexity of the former compared to the latter. Even after removing the outliers, representing the worst-performing hybrid meta-GGA DFAs (M06-HF and M06-HF-D3(0),<sup>95</sup> global hybrids with 100% HF exchange), the hybrid meta-GGA class performs slightly worse (0.077 eV MAE, 0.208 MRAE) than the hybrid GGA DFAs (0.071 eV MAE, 0.204 MRAE) on average. Another interesting distinction between hybrid and pure DFAs arises when analyzing their accuracy for the forward reaction versus the reverse reaction, i.e., the addition of water versus the elimination of water

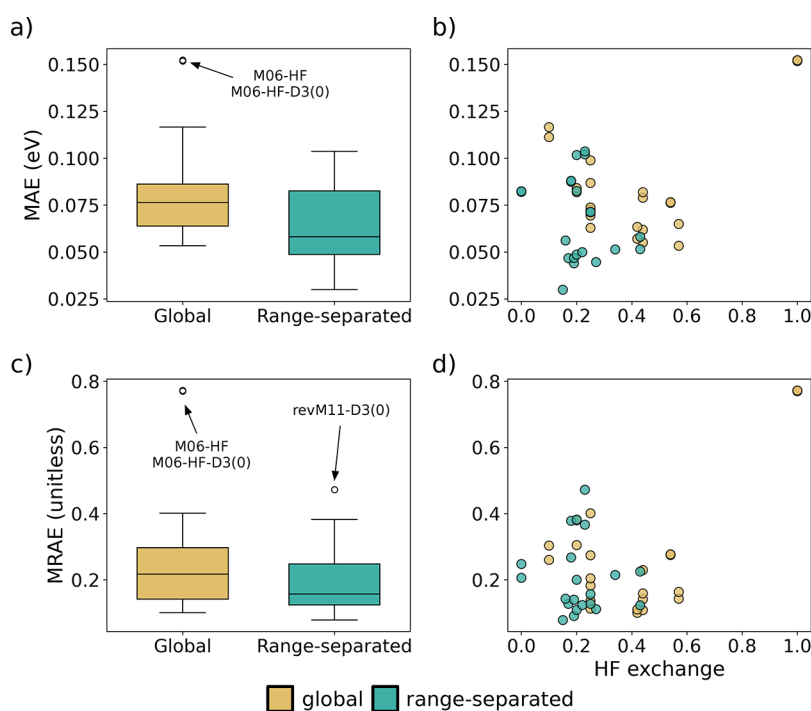


**Figure 2.** Performance of global and range-separated hybrid DFAs in calculating hydrolysis energy barriers from fixed SCAN-optimized geometries. (a) Box plot of MAE for global and range-separated hybrid DFAs; (b) scatter plot of MAE data, showing the effect of HF exchange fraction on accuracy; (c) box plot of MRAE for global and range-separated hybrid DFAs; (d) scatter plot of MRAE data, showing the effect of HF exchange fraction on accuracy. For range-separated hybrids, the *x*-axis of the scatter plots in panels b and d is the fraction of short-range exchange; for global hybrids, it is the global HF exchange fraction.

(Figure S4). Pure GGA and meta-GGA DFAs are significantly less accurate for the reverse reaction than they are for the forward reaction (0.099 eV  $\Delta$  Mean MAE, 0.041 eV  $\Delta$  Mean MAE) while the hybrid GGA and hybrid Meta-GGA DFAs display similar performance (0.001 eV  $\Delta$  Mean MAE, 0.017 eV  $\Delta$  Mean MAE).

The range of MAE values observed for meta-GGA and hybrid meta-GGA DFAs (Figure 1a) is particularly wide. This can be attributed to a very small number of poor-performing DFAs. In the case of the meta-GGA DFAs, the upper bound of the MAE range is populated by TPSS<sup>79</sup> and TPSS-D3(BJ).<sup>69,79</sup> These DFAs are known to underbind dispersion-bound compounds,<sup>106</sup> which are exemplified by the reaction complexes and transition states considered here. In addition to the M06-HF and M06-HF-D3(0) which we have already discussed, TPSSh<sup>99</sup> and TPSSh-D3(BJ)<sup>69,99</sup> exhibit high MAE among the hybrid meta-GGA DFAs. With a similar functional form to TPSS, it is perhaps somewhat unsurprising that TPSSh and its derivative perform poorly in the prediction of barrier heights. Although M06-HF was primarily designed for time-dependent DFT (TDDFT) calculations,<sup>120</sup> it was parametrized on several barrier height data sets. It is therefore counter-intuitive that M06-HF and M06-HF-D3(0) appear to pathologically fail to predict hydrolysis energy barriers.

While hybrid DFAs generally perform better than their pure counterparts without the inclusion of HF exchange, not all hybrid DFAs are created equal. The hybrid DFAs included in this benchmark study have fractions of short-range HF exchange ranging from 0 (LRC- $\omega$ PBE and LRC- $\omega$ PBE-D3(BJ)) to 1 (M06-HF and M06-HF-D3(0)); in addition, we included both global hybrid DFAs, with HF exchange included uniformly through space, and range-separated hybrid DFAs, which aim to more rigorously eliminate self-interaction

errors through the separation of the exchange into short-range and long-range terms. In most cases, the range-separated hybrids considered here perform better than global hybrids; this is especially true when considering the MAE (Figure 2a). It is worth noting that 8 of the top 10 ranked DFAs in Table 3 are range-separated hybrids (MN15 and BMK-D3(BJ) are global hybrids). Several of these high-performing range-separated hybrids highlight the improvement that range separation adds. CAM-B3LYP-D3(0) and  $\omega$ M06-D3 both transform a poorly performing DFA (B3LYP and M06-2X, respectively) to one that ranks in the top 5, with MAE improvements of 0.038 and 0.028 eV over the DFAs they were based on, respectively. These DFAs also all take significantly different approaches to range separation. For example, the long-range HF exchange component of the range separation operator varies significantly— $\omega$ M06-D3 uses 100% and CAM-B3LYP uses 65%. Despite these differences in functional form, reparameterization of the DFAs with the inclusion of range separation elevates their performances to a similar extent. Further emphasizing that different approaches to the functional form of range separation can lead to similarly positive results, the fraction of short-range HF exchange seems to have little effect on the accuracy of the range-separated hybrids in this benchmark set (Figure 2b,d). Based on these findings, for predictions of hydrolysis kinetics, range-separated hybrids should be preferred. If a global hybrid must be used, moderate to high fraction of HF exchange may be desirable.

Many of the DFAs that perform well on the BH2O-36 benchmark include a dispersion correction. Among the top 10 DFAs, two ( $\omega$ B97M-V and  $\omega$ B97X-V) use VV10, five (CAM-B3LYP-D3(0), M06-SX-D3(BJ),  $\omega$ M06-D3,  $\omega$ B97X-D3, and BMK-D3(BJ)) use the D3 empirical correction, and one ( $\omega$ B97X-D) uses D2. It is therefore worth asking whether

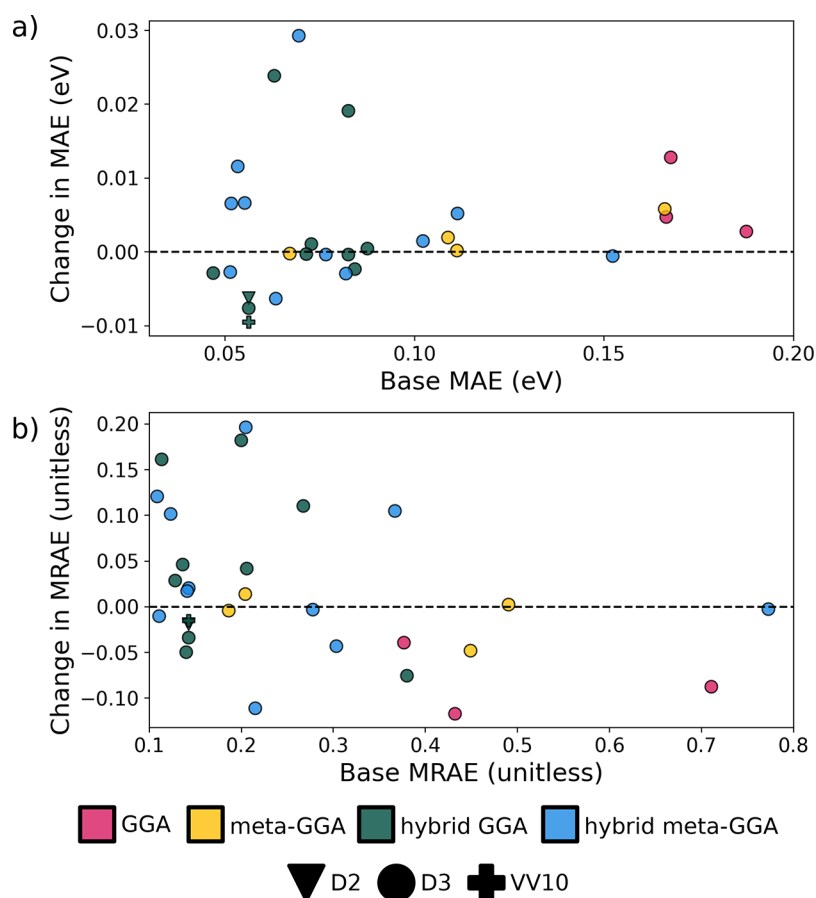


**Figure 3.** Comparing MAE (a) and MRAE (b) of DFAs with various dispersion corrections, including the empirical D2 and D3 corrections as well as the nonlocal correlation DFA VV10. The  $x$ -axes are the MAE or MRAE of the nondispersion-corrected DFA, and the  $y$ -axes are the changes in MAE or MRAE for the dispersion-corrected DFAs relative to the noncorrected values. A change in MAE or MRAE of 0 indicates that dispersion correction has no effect on the prediction error, on average. Negative values indicate an improvement over the nondispersion-corrected DFA, while positive values indicate that the dispersion correction has a detrimental effect on the error.

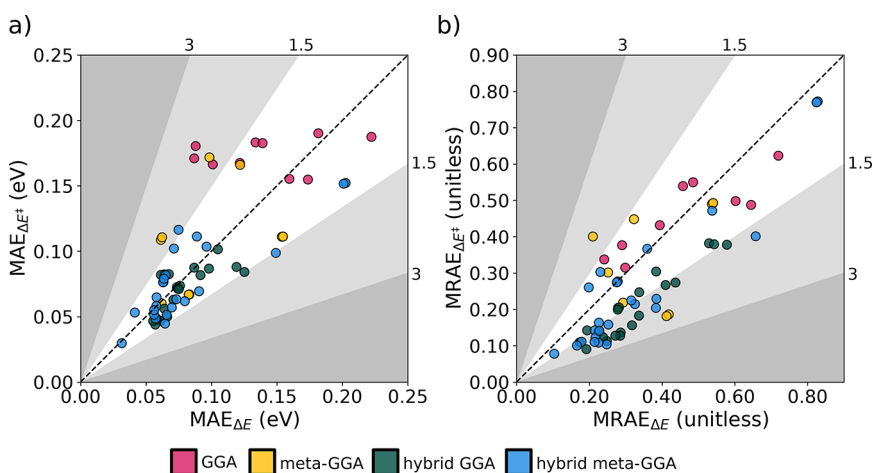


**Figure 4.** Error in predicted energy barrier  $\Delta E^\ddagger$  versus reaction energy  $\Delta E$  in terms of MAE (a) and MRAE (b). The dashed line, with the equation  $\text{Error}_{\Delta E^\ddagger} = \text{Error}_{\Delta E}$ , indicates DFAs that have equal error for reaction energies and energy barriers. Boundaries between the gray regions indicate deviations from the  $\text{Error}_{\Delta E^\ddagger} = \text{Error}_{\Delta E}$  by factors of 1.5 and 3, as well as their reciprocals, as noted on the plots.

dispersion corrections, in general, improve the accuracy of DFT-predicted hydrolysis barrier heights.

Since transition states often involve the formation and/or breaking of bonds, with interatomic interactions on length scales significantly longer than typical ground-state bond lengths, it would follow logically that the long-range energy

terms provided by dispersion corrections would improve calculations of transition-state energies and, therefore, barrier heights. As Figure 3 shows, this does not appear to be the case for the BH2O-36 benchmark set. In terms of MAE (Figure 3a), dispersion corrections often lead to small changes on the order of meV. While modest improvement is seen for some DFAs

(notably, those based on  $\omega$ B97X and BMK), the addition of a D3 correction can lead to significantly *higher* error (e.g., for PBE,<sup>68</sup> mPW91,<sup>73</sup> M08-SO,<sup>96</sup> and SCAN<sup>100</sup>). We note that  $\omega$ B97X-D,  $\omega$ B97X-D3, and  $\omega$ B97X-V were all specifically trained to use a dispersion correction, which is not true for most dispersion-corrected DFAs tested here. The changes in MRAE (Figure 3b) caused by the addition of dispersion corrections are more significant, but once again, uniform improvement is not observed upon the addition of dispersion corrections. In the Supporting Information (Tables S6 and S7), we likewise find that the DFT-D4 dispersion correction does not significantly improve over nondispersion-corrected DFAs or over previous dispersion corrections like D2 and D3. These findings are consistent with conclusions from a previous benchmark for the hydrolysis of glycosidic bonds.<sup>67</sup>

While our focus in this work is on reaction energy barriers, it is worth pausing to consider reaction thermochemistry, as both reaction energies  $\Delta E$  and energy barriers  $\Delta E^\ddagger$  are required for most practical applications (e.g., constructing energy diagrams or performing microkinetic modeling). The MAE and MRAE for  $\Delta E^\ddagger$  versus those for  $\Delta E$  are shown in Figure 4.

Analyzing the MAE (Figure 4a), we find that many pure DFAs—and almost all GGA DFAs considered here—are considerably worse at predicting energy barriers than reaction energies when benchmarked on BH2O-36. While underperformance on energy barriers is not unique to pure DFAs, hybrids in general seem to be better behaved and follow a more linear trend, adhering more or less closely to the line  $\text{Error}_{\Delta E^\ddagger} = \text{Error}_{\Delta E}$ . This provides further evidence that hybrid DFAs should be strongly favored over their pure counterparts. Further, the finding that many DFAs that can reasonably predict hydrolysis reaction energies fail when predicting related energy barriers highlights the necessity of benchmarks specific to chemical kinetics. The MRAE for  $\Delta E$  and  $\Delta E^\ddagger$  are more similar (Figure 4b) than the MAE. Most DFAs (and essentially all hybrid DFAs) have an  $\text{MRAE}_{\Delta E^\ddagger}$  that is lower than the respective  $\text{MRAE}_{\Delta E}$ . This is unsurprising, as the reference reaction energies are on average smaller in magnitude compared to the reference energy barriers ( $|\Delta E|_{\text{ref,avg}} = 0.022$  eV,  $\Delta E^\ddagger_{\text{ref,avg}} = 0.035$  eV). The overall performance of the highest-ranking DFAs for thermodynamics does not significantly differ from the kinetics and the comparisons across DFA classes largely remain the same, except for an improved performance of meta-GGAs compared to hybrid-GGAs and hybrid meta-GGAs (Figure S3 and Table S4).

## CONCLUSION

In this work, we presented a new data set, BH2O-36, which can be used to assess the ability of DFAs to predict the energy barriers of diverse hydrolysis reactions. Using BH2O-36, we analyzed 63 DFAs, including GGA, meta-GGA, and hybrid DFAs (the latter group including GGA, meta-GGA, global, and range-separated hybrids). The GGA DFAs we tested performed poorly on this benchmark (with the exception of the anomalous performance of the DFT-D4-corrected B97-D4), and therefore we would not generally recommend using GGA DFA in studies of hydrolysis kinetics or reaction barriers. When dealing with large systems or in cases where computational resources are otherwise constrained, several meta-GGA DFAs could be reasonably employed. In particular, we recommend the Minnesota DFAs MN12-L and MN12-L-D3(BJ), as well as the rVV10-corrected DFA B97M-rV. When

computational cost is not a significant obstacle, we recommend the use of range-separated hybrid DFAs broadly. The  $\omega$ B97M-V and CAM-B3LYP-D3(0) range-separated hybrid DFAs show the best performance within our benchmark set, but many other range-separated hybrids (e.g., M06-SX-D3(BJ)  $\omega$ M06-D3,  $\omega$ B97X-D3,  $\omega$ B97X-V) are also well-performing contenders. These recommended range-separated hybrid DFAs are 1.5–2.3 times slower in their single-point energy calculations than the recommended meta-GGAs (Figure S5).

Considering DFA design, we found that dispersion correction does not systematically improve the accuracy of DFAs in predicting hydrolysis energy barriers, and in many cases, the introduction of a dispersion correction leads to significantly higher error. While this may be counterintuitive, considering the role of long-range interactions at transition states, this finding suggests that dispersion corrections should not be blindly applied in studies of hydrolysis reactions specifically, and perhaps of reaction mechanisms more generally. Likewise, although hybrid DFAs typically outperform pure DFAs on the BH2O-36 benchmark, we found that among hybrid DFAs, there is no strong indication that an increase in the fraction of short-range HF exchange leads to lower MAE or MRAE. This is not surprising for range-separated hybrids, which are all of the top-performing DFAs in this study, as they depend significantly on the interplay of several parameters tuned in their creation. For example, the  $\omega$  parameter controlling the partitioning of the HF exchange<sup>93</sup> and the strength of the dispersion correction included in the parametrization,<sup>92</sup> are both known to lead to significant differences in the fraction of short-range HF exchange. We therefore emphasize that there is no single key to choosing a DFA for reaction kinetics, and benchmarks are essential for determining the appropriate DFA for particular tasks.

While particularly designed to assist in computational studies of aqueous chemistry and reactivity, the BH2O-36 can supplement other energy barrier and kinetic benchmark sets in order to aid in the design of new DFAs and semiempirical quantum chemical methods.

## ASSOCIATED CONTENT

### Data Availability Statement

All data used in this study, including reference values calculated at the CCSD(T)/CBS level of theory, as well as all code used to set up calculations, parse and process data, perform analysis, and generate plots for figures, is included in the “hydrobench” repository on Github (<https://github.com/espottesmith/hydrobench>).

### Supporting Information

The Supporting Information is available free of charge at <https://pubs.acs.org/doi/10.1021/acs.jctc.3c00176>.

Reference energy barriers calculated with a CCSD(T)/CBS approximation; analysis of signed errors for the prediction of hydrolysis energy barriers; analysis of MAE and MRAE for structures optimized using a different DFA ( $\omega$ B97M-V); analysis of MAE and MRAE for prediction of reaction energies  $\Delta E$ ; analysis of MAE and MRAE for a subset of DFAs with the addition of the DFT-D4 dispersion correction; analysis of MAE and MRAE organized by reaction class, including by the forward versus reverse reactions; benchmark of computational cost in terms of walltime for single-point energy evaluations (PDF)

## AUTHOR INFORMATION

### Corresponding Author

Kristin Aslaug Persson – Department of Materials Science and Engineering, University of California, Berkeley, California 94720, United States; Molecular Foundry, Lawrence Berkeley National Laboratory, Berkeley, California 94720, United States; [orcid.org/0000-0003-2495-5509](https://orcid.org/0000-0003-2495-5509); Email: [kapersson@lbl.gov](mailto:kapersson@lbl.gov)

### Authors

Alexander Rizzolo Epstein – Department of Materials Science and Engineering, University of California, Berkeley, California 94720, United States; [orcid.org/0000-0002-9914-2388](https://orcid.org/0000-0002-9914-2388)

Evan Walter Clark Spotte-Smith – Department of Materials Science and Engineering, University of California, Berkeley, California 94720, United States; Materials Science Division, Lawrence Berkeley National Laboratory, Berkeley, California 94720, United States; [orcid.org/0000-0003-1554-197X](https://orcid.org/0000-0003-1554-197X)

Maxwell C. Venetos – Department of Materials Science and Engineering, University of California, Berkeley, California 94720, United States; Materials Science Division, Lawrence Berkeley National Laboratory, Berkeley, California 94720, United States; [orcid.org/0000-0003-3468-2006](https://orcid.org/0000-0003-3468-2006)

Oxana Andriuc – Department of Chemistry, University of California, Berkeley, California 94720, United States; Chemical Sciences Division, Lawrence Berkeley National Laboratory, Berkeley, California 94720, United States; [orcid.org/0000-0002-4011-3339](https://orcid.org/0000-0002-4011-3339)

Complete contact information is available at:  
<https://pubs.acs.org/10.1021/acs.jctc.3c00176>

### Author Contributions

<sup>†</sup>A.R.E. and E.W.C.S.-S. contributed equally to this work. Co-first author order is alphabetical by last name and does not reflect relative contributions. A.R.E. and E.W.C.S.-S. both have the right to list their names first when presenting this research or listing it in their CVs. Conceptualization: A.R.E., E.W.C.S.-S., M.C.V.; data curation: A.R.E., E.W.C.S.-S.; formal analysis: A.R.E., E.W.C.S.-S., M.C.V., O.A.; funding: A.R.E., E.W.C.S.-S., M.C.V., K.A.P.; investigation: A.R.E., E.W.C.S.-S., M.C.V., O.A.; methodology: A.R.E., E.W.C.S.-S., M.C.V.; project administration: A.R.E.; resources: K.A.P.; software: A.R.E., E.W.C.S.-S.; supervision: K.A.P.; validation: E.W.C.S.-S.; visualization: A.R.E., E.W.C.S.-S., M.C.V.; writing: original draft - A.R.E., E.W.C.S.-S., M.C.V., O.A.; writing - review and editing: all authors.

### Notes

The authors declare no competing financial interest.

## ACKNOWLEDGMENTS

E.W.C.S.-S. is supported by the Kavli Energy Nanoscience Institute Philomathia Graduate Student Fellowship. A.R.E. is supported by the National Science Foundation Graduate Research Fellowship under Grant No. DGE 1752814. O.A. is supported by the Liquid Sunlight Alliance, which is supported by the U.S. Department of Energy, Office of Science, Office of Basic Energy Sciences, Fuels from Sunlight Hub under Award Number DE-SC0021266. Data for this study was produced using computational resources provided by the National Energy Research Scientific Computing Center (NERSC), a U.S. Department of Energy Office of Science User Facility

under Contract No. DE-AC02-05CH11231, the Eagle and Swift HPC systems at the National Renewable Energy Laboratory (NREL), and the Lawrence HPC cluster at Lawrence Berkeley National Laboratory. The authors thank Samuel M. Blau for useful discussions.

## REFERENCES

- (1) Weber, J.; Senior, A. E. ATP synthase: what we know about ATP hydrolysis and what we do not know about ATP synthesis. *Biochimica et Biophysica Acta (BBA) - Bioenergetics* **2000**, *1458*, 300–309.
- (2) Korn, E. D.; Carlier, M.-F.; Pantaloni, D. Actin Polymerization and ATP Hydrolysis. *Science* **1987**, *238*, 638–644.
- (3) Mellouki, A.; Wallington, T. J.; Chen, J. Atmospheric Chemistry of Oxygenated Volatile Organic Compounds: Impacts on Air Quality and Climate. *Chemical Reviews* **2015**, *115*, 3984–4014.
- (4) Mabey, W.; Mill, T. Critical review of hydrolysis of organic compounds in water under environmental conditions. *J. Phys. Chem. Ref. Data* **1978**, *7*, 383–415.
- (5) Pehkonen, S. O.; Zhang, Q. The Degradation of Organophosphorus Pesticides in Natural Waters: A Critical Review. *Critical Reviews in Environmental Science and Technology* **2002**, *32*, 17–72.
- (6) Li, J.; Mooney, D. J. Designing hydrogels for controlled drug delivery. *Nature Reviews Materials* **2016**, *1*, 16071.
- (7) Sahin, U.; Karikó, K.; Türeci, O. mRNA-based therapeutics — developing a new class of drugs. *Nature Reviews Drug Discovery* **2014**, *13*, 759–780.
- (8) Vargiu, A. V.; Robertazzi, A.; Magistrato, A.; Ruggerone, P.; Carloni, P. The Hydrolysis Mechanism of the Anticancer Ruthenium Drugs NAMI-A and ICR Investigated by DFT-PCM Calculations. *The Journal of Physical Chemistry B* **2008**, *112*, 4401–4409.
- (9) Barber, W. P. F. Thermal hydrolysis for sewage treatment: A critical review. *Water Res.* **2016**, *104*, 53–71.
- (10) Shen, M.; Cao, H.; Robertson, M. L. Hydrolysis and solvolysis as benign routes for the end-of-life management of thermoset polymer waste. *Annu. Rev. Chem. Biomol. Eng.* **2020**, *11*, 183–201.
- (11) Helms, B. A. Polydiketoenamines for a Circular Plastics Economy. *Acc. Chem. Res.* **2022**, *55*, 2753.
- (12) Cordes, E.; Bull, H. Mechanism and catalysis for hydrolysis of acetals, ketals, and ortho esters. *Chem. Rev.* **1974**, *74*, 581–603.
- (13) Brown, R. S.; Bennet, A. J.; Slebocka-Tilk, H. Recent perspectives concerning the mechanism of H<sub>3</sub>O<sup>+</sup>- and hydroxide-promoted amide hydrolysis. *Acc. Chem. Res.* **1992**, *25*, 481–488.
- (14) Larson, L. J.; Kuno, M.; Tao, F.-M. Hydrolysis of sulfur trioxide to form sulfuric acid in small water clusters. *The Journal of Chemical Physics* **2000**, *112*, 8830–8838.
- (15) Gunaydin, H.; Houk, K. N. Molecular Dynamics Prediction of the Mechanism of Ester Hydrolysis in Water. *J. Am. Chem. Soc.* **2008**, *130*, 15232–15233.
- (16) Kamerlin, S. C. L.; Haranczyk, M.; Warshel, A. Are Mixed Explicit/Implicit Solvation Models Reliable for Studying Phosphate Hydrolysis? A Comparative Study of Continuum, Explicit and Mixed Solvation Models. *ChemPhysChem* **2009**, *10*, 1125–1134.
- (17) Brás, N. F.; Fernandes, P. A.; Ramos, M. J. QM/MM Studies on the  $\beta$  - Galactosidase Catalytic Mechanism: Hydrolysis and Transglycosylation Reactions. *Journal of Chemical Theory and Computation* **2010**, *6*, 421–433.
- (18) Freedman, H.; Laino, T.; Curioni, A. Reaction Dynamics of ATP Hydrolysis in Actin Determined by ab Initio Molecular Dynamics Simulations. *Journal of Chemical Theory and Computation* **2012**, *8*, 3373–3383.
- (19) Robins, L. I.; Fogle, E. J.; Marlier, J. F. Mechanistic investigations of the hydrolysis of amides, oxoesters and thioesters via kinetic isotope effects and positional isotope exchange. *Biochimica et Biophysica Acta (BBA) - Proteins and Proteomics* **2015**, *1854*, 1756–1767.
- (20) Galib, M.; Limmer, D. T. Reactive uptake of N<sub>2</sub>O<sub>5</sub> by atmospheric aerosol is dominated by interfacial processes. *Science* **2021**, *371*, 921–925.

- (21) Glancy, J. H.; Lee, D. M.; Read, E. O.; Williams, I. H. Computational simulation of mechanism and isotope effects on acetal hydrolysis as a model for glycoside hydrolysis. *Pure Appl. Chem.* **2020**, *92*, 75–84.
- (22) Labet, V.; Grand, A.; Morell, C.; Cadet, J.; Eriksson, L. A. Proton catalyzed hydrolytic deamination of cytosine: a computational study. *Theor. Chem. Acc.* **2008**, *120*, 429–435.
- (23) Cheshmedzhieva, D.; Ilieva, S.; Hadjieva, B.; Galabov, B. The mechanism of alkaline hydrolysis of amides: a comparative computational and experimental study of the hydrolysis of N-methylacetamide, N-methylbenzamide, and acetanilide. *J. Phys. Org. Chem.* **2009**, *22*, 619–631.
- (24) Gorb, L.; Asensio, A.; Tuñón, I.; Ruiz-López, M. F. The Mechanism of Formamide Hydrolysis in Water from Ab Initio Calculations and Simulations. *Chem.—Eur. J.* **2005**, *11*, 6743–6753.
- (25) Xiong, Y.; Zhan, C.-G. Theoretical Studies of the Transition-State Structures and Free Energy Barriers for Base-Catalyzed Hydrolysis of Amides. *J. Phys. Chem. A* **2006**, *110*, 12644–12652.
- (26) García Martínez, A.; de la Moya Cerero, S.; Osío Barcina, J.; Moreno Jiménez, F.; Lora Maroto, B. The Mechanism of Hydrolysis of Aryldiazonium Ions Revisited: Marcus Theory vs. Canonical Variational Transition State Theory: Hydrolysis of Aryldiazonium Ions Revisited. *Eur. J. Org. Chem.* **2013**, *2013*, 6098–6107.
- (27) Shi, H.; Huang, X.; Liu, G.; Yu, K.; Xu, C.; Li, W.; Zeng, B.; Tang, Y. The role of benzoic acid in proline-catalyzed asymmetric Michael addition: A density functional theory study. *Int. J. Quantum Chem.* **2013**, *113*, 1339–1348.
- (28) Ren, J.; Li, G.-Y.; Shen, L.; Zhang, G.-L.; Nafie, L. A.; Zhu, H.-J. Challenges in the assignment of relative and absolute configurations of complex molecules: computation can resolve conflicts between theory and experiment. *Tetrahedron* **2013**, *69*, 10351–10356.
- (29) Erdemir, S.; Malkondu, S.; Kararkurt, S. Synthesis and cell imaging studies of an unusual “OFF–ON” fluorescent sensor containing a triazole unit for Al<sup>3+</sup> detection via selective imine hydrolysis. *Analyst* **2020**, *145*, 3725–3731.
- (30) Gómez-Bombarelli, R.; Calle, E.; Casado, J. Mechanisms of Lactone Hydrolysis in Neutral and Alkaline Conditions. *J. Org. Chem.* **2013**, *78*, 6868–6879.
- (31) Cheshmedzhieva, D.; Ilieva, S.; Galabov, B. Computational study of the alkaline hydrolysis of acetanilide. *Journal of Molecular Structure: THEOCHEM* **2004**, *681*, 105–112.
- (32) Ivanova, E. V.; Muchall, H. M. From Inert to Explosive, The Hydrolytic Reactivity of R-NSO Compounds Understood: A Computational Study. *J. Phys. Chem. A* **2011**, *115*, 3095–3105.
- (33) Ivanova, E. V.; Muchall, H. M. Hydrolysis of N-Sulfinylamines and Isocyanates: A Computational Comparison. *J. Phys. Chem. A* **2007**, *111*, 10824–10833.
- (34) Rosta, E.; Kamerlin, S. C. L.; Warshel, A. On the Interpretation of the Observed Linear Free Energy Relationship in Phosphate Hydrolysis: A Thorough Computational Study of Phosphate Diester Hydrolysis in Solution. *Biochemistry* **2008**, *47*, 3725–3735.
- (35) Galabov, B.; Cheshmedzhieva, D.; Ilieva, S.; Hadjieva, B. Computational Study of the Reactivity of N-Phenylacetamides in the Alkaline Hydrolysis Reaction. *J. Phys. Chem. A* **2004**, *108*, 11457–11462.
- (36) Janesko, B. G. Acid-catalyzed hydrolysis of lignin β-O-4 linkages in ionic liquid solvents: a computational mechanistic study. *Phys. Chem. Chem. Phys.* **2014**, *16*, 5423.
- (37) Karaman, R. Analyzing the efficiency in intramolecular amide hydrolysis of Kirby's N-alkylmaleamic acids – A computational approach. *Computational and Theoretical Chemistry* **2011**, *974*, 133–142.
- (38) Li, L.; Lelyveld, V. S.; Prywes, N.; Szostak, J. W. Experimental and Computational Evidence for a Loose Transition State in Phosphoroimidazolide Hydrolysis. *J. Am. Chem. Soc.* **2016**, *138*, 3986–3989.
- (39) Ribaldo, G.; Bortoli, M.; Oselladore, E.; Ongaro, A.; Gianoncelli, A.; Zagotto, G.; Orian, L. Selenoxide Elimination Triggers Enamine Hydrolysis to Primary and Secondary Amines: A Combined Experimental and Theoretical Investigation. *Molecules* **2021**, *26*, 2770.
- (40) Berkefeld, A.; Guerra, C. F.; Bertermann, R.; Troegel, D.; Daiß, J. O.; Stohrer, J.; Bickelhaupt, F. M.; Tacke, R. Silicon α-Effect: A Systematic Experimental and Computational Study of the Hydrolysis of C<sup>α</sup>- and C<sup>γ</sup>-Functionalized Alkoxytriorganylsilanes of the Formula Type ROSiMe<sub>2</sub>(CH<sub>2</sub>)<sub>n</sub>X (R = Me, Et; n = 1, 3; X = Functional Group). *Organometallics* **2014**, *33*, 2721–2737.
- (41) Nikbin, N.; Caratzoulas, S.; Vlachos, D. G. On the Brønsted Acid-Catalyzed Homogeneous Hydrolysis of Furans. *ChemSusChem* **2013**, *6*, 2066–2068.
- (42) Szeler, K.; Williams, N. H.; Hengge, A. C.; Kamerlin, S. C. L. Modeling the Alkaline Hydrolysis of Diaryl Sulfate Diesters: A Mechanistic Study. *J. Org. Chem.* **2020**, *85*, 6489–6497.
- (43) Yang, L.; Feng, J.; Zhang, W.; Qu, J.-e. Experimental and computational study on hydrolysis and condensation kinetics of γ-glycidoxypolytrimethoxysilane (γ-GPS). *Appl. Surf. Sci.* **2010**, *257*, 990–996.
- (44) Kabanda, M. M.; Tran, V. T.; Tran, Q. T.; Ebenso, E. E. A computational study of pyrazinamide: Tautomerism, acid–base properties, micro-solvation effects and acid hydrolysis mechanism. *Computational and Theoretical Chemistry* **2014**, *1046*, 30–41.
- (45) Goodell, J. R.; Svensson, B.; Ferguson, D. M. Spectrophotometric Determination and Computational Evaluation of the Rates of Hydrolysis of 9-Amino-Substituted Acridines. *J. Chem. Inf. Model.* **2006**, *46*, 876–883.
- (46) Demarteau, J.; Epstein, A. R.; Christensen, P. R.; Abubekero, M.; Wang, H.; Teat, S. J.; Seguin, T. J.; Chan, C. W.; Scown, C. D.; Russell, T. P.; Keasling, J. D.; Persson, K. A.; Helms, B. A. Circularity in mixed-plastic chemical recycling enabled by variable rates of polydiketoenamine hydrolysis. *Science Advances* **2022**, *8*, eabp8823.
- (47) Bakowies, D.; Kollman, P. A. Theoretical Study of Base-Catalyzed Amide Hydrolysis: Gas- and Aqueous-Phase Hydrolysis of Formamide. *J. Am. Chem. Soc.* **1999**, *121*, 5712–5726.
- (48) Hall, N. E.; Smith, B. J. High-Level ab Initio Molecular Orbital Calculations of Imine Formation. *J. Phys. Chem. A* **1998**, *102*, 4930–4938.
- (49) Antonczak, S.; Ruiz-Lopez, M. F.; Rivail, J. L. Ab Initio Analysis of Water-Assisted Reaction Mechanisms in Amide Hydrolysis. *J. Am. Chem. Soc.* **1994**, *116*, 3912–3921.
- (50) Lynch, B. J.; Zhao, Y.; Truhlar, D. G. Effectiveness of Diffuse Basis Functions for Calculating Relative Energies by Density Functional Theory. *The Journal of Physical Chemistry A* **2003**, *107*, 1384–1388.
- (51) Zhao, Y.; González-García, N.; Truhlar, D. G. Benchmark Database of Barrier Heights for Heavy Atom Transfer, Nucleophilic Substitution, Association, and Unimolecular Reactions and Its Use to Test Theoretical Methods. *J. Phys. Chem. A* **2005**, *109*, 2012–2018.
- (52) Karton, A.; Gruzman, D.; Martin, J. M. L. Benchmark Thermochemistry of the C<sub>n</sub>H<sub>2n+2</sub> Alkane Isomers (n = 2–8) and Performance of DFT and Composite Ab Initio Methods for Dispersion-Driven Isomeric Equilibria. *The Journal of Physical Chemistry A* **2009**, *113*, 8434–8447.
- (53) Goerigk, L.; Grimme, S. A General Database for Main Group Thermochemistry, Kinetics, and Noncovalent Interactions - Assessment of Common and Re-parameterized (meta-)GGA Density Functionals. *Journal of Chemical Theory and Computation* **2010**, *6*, 107–126.
- (54) Karton, A.; Daon, S.; Martin, J. M. L. W4–11: A high-confidence benchmark dataset for computational thermochemistry derived from first-principles W4 data. *Chem. Phys. Lett.* **2011**, *510*, 165–178.
- (55) Goerigk, L.; Grimme, S. Efficient and Accurate Double-Hybrid-Meta-GGA Density Functionals—Evaluation with the Extended GMTKN30 Database for General Main Group Thermochemistry, Kinetics, and Noncovalent Interactions. *Journal of Chemical Theory and Computation* **2011**, *7*, 291–309.

- (56) Karton, A.; Schreiner, P. R.; Martin, J. M. L. Heats of formation of platonic hydrocarbon cages by means of high-level thermochemical procedures. *J. Comput. Chem.* **2016**, *37*, 49–58.
- (57) O'Reilly, R. J.; Karton, A. A dataset of highly accurate homolytic N-Br bond dissociation energies obtained by Means of W2 theory. *Int. J. Quantum Chem.* **2016**, *116*, 52–60.
- (58) Maurer, L. R.; Bursch, M.; Grimme, S.; Hansen, A. Assessing Density Functional Theory for Chemically Relevant Open-Shell Transition Metal Reactions. *J. Chem. Theory Comput.* **2021**, *17*, 6134.
- (59) Zheng, J.; Zhao, Y.; Truhlar, D. G. Representative Benchmark Suites for Barrier Heights of Diverse Reaction Types and Assessment of Electronic Structure Methods for Thermochemical Kinetics. *Journal of Chemical Theory and Computation* **2007**, *3*, 569–582.
- (60) Karton, A.; Tarnopolsky, A.; Lamère, J.-F.; Schatz, G. C.; Martin, J. M. L. Highly Accurate First-Principles Benchmark Data Sets for the Parametrization and Validation of Density Functional and Other Approximate Methods. Derivation of a Robust, Generally Applicable, Double-Hybrid Functional for Thermochemistry and Thermochemical Kinetics. *The Journal of Physical Chemistry A* **2008**, *112*, 12868–12886.
- (61) Karton, A.; O'Reilly, R. J.; Radom, L. Assessment of Theoretical Procedures for Calculating Barrier Heights for a Diverse Set of Water-Catalyzed Proton-Transfer Reactions. *J. Phys. Chem. A* **2012**, *116*, 4211–4221.
- (62) Karton, A.; O'Reilly, R. J.; Chan, B.; Radom, L. Determination of Barrier Heights for Proton Exchange in Small Water, Ammonia, and Hydrogen Fluoride Clusters with G4(MP2)-Type, MPn, and SCS-MPn Procedures—A Caveat. *Journal of Chemical Theory and Computation* **2012**, *8*, 3128–3136.
- (63) Yu, L.-J.; Sarrami, F.; O'Reilly, R. J.; Karton, A. Reaction barrier heights for cycloreversion of heterocyclic rings: An Achilles' heel for DFT and standard ab initio procedures. *Chem. Phys.* **2015**, *458*, 1–8.
- (64) Karton, A.; Goerigk, L. Accurate reaction barrier heights of pericyclic reactions: Surprisingly large deviations for the CBS-QB3 composite method and their consequences in DFT benchmark studies. *J. Comput. Chem.* **2015**, *36*, 622–632.
- (65) Prasad, V. K.; Pei, Z.; Edelmann, S.; Otero-de-la Roza, A.; DiLabio, G. A. BH9, a New Comprehensive Benchmark Data Set for Barrier Heights and Reaction Energies: Assessment of Density Functional Approximations and Basis Set Incompleteness Potentials. *J. Chem. Theory Comput.* **2022**, *18*, 151–166.
- (66) Ribeiro, A. J. M.; Ramos, M. J.; Fernandes, P. A. Benchmarking of DFT Functionals for the Hydrolysis of Phosphodiester Bonds. *J. Chem. Theory Comput.* **2010**, *6*, 2281–2292.
- (67) Pereira, A. T.; Ribeiro, A. J. M.; Fernandes, P. A.; Ramos, M. J. Benchmarking of density functionals for the kinetics and thermodynamics of the hydrolysis of glycosidic bonds catalyzed by glycosidases. *Int. J. Quantum Chem.* **2017**, *117*, No. e25409.
- (68) Perdew, J. P.; Burke, K.; Ernzerhof, M. Generalized Gradient Approximation Made Simple. *Phys. Rev. Lett.* **1996**, *77*, 3865–3868.
- (69) Grimme, S.; Ehrlich, S.; Goerigk, L. Effect of the damping function in dispersion corrected density functional theory. *J. Comput. Chem.* **2011**, *32*, 1456–1465.
- (70) Becke, A. D. Density-functional exchange-energy approximation with correct asymptotic behavior. *Phys. Rev. A* **1988**, *38*, 3098–3100.
- (71) Lee, C.; Yang, W.; Parr, R. G. Development of the Colle-Salvetti correlation-energy formula into a functional of the electron density. *Phys. Rev. B* **1988**, *37*, 785.
- (72) Grimme, S. Semiempirical GGA-type density functional constructed with a long-range dispersion correction. *J. Comput. Chem.* **2006**, *27*, 1787–1799.
- (73) Adamo, C.; Barone, V. Exchange functionals with improved long-range behavior and adiabatic connection methods without adjustable parameters: The mPW and mPW1PW models. *J. Chem. Phys.* **1998**, *108*, 664–675.
- (74) Vydrov, O. A.; Van Voorhis, T. Nonlocal van der Waals density functional: The simpler the better. *J. Chem. Phys.* **2010**, *133*, 244103.
- (75) Sabatini, R.; Gorni, T.; de Gironcoli, S. Nonlocal van der Waals density functional made simple and efficient. *Phys. Rev. B* **2013**, *87*, 041108.
- (76) Zhao, Y.; Truhlar, D. G. A new local density functional for main-group thermochemistry, transition metal bonding, thermochemical kinetics, and noncovalent interactions. *J. Chem. Phys.* **2006**, *125*, 194101.
- (77) Grimme, S.; Antony, J.; Ehrlich, S.; Krieg, H. A consistent and accurate ab initio parametrization of density functional dispersion correction (DFT-D) for the 94 elements H-Pu. *J. Chem. Phys.* **2010**, *132*, 154104.
- (78) Sun, J.; Ruzsinszky, A.; Perdew, J. Strongly Constrained and Appropriately Normed Semilocal Density Functional. *Phys. Rev. Lett.* **2015**, *115*, 036402.
- (79) Tao, J.; Perdew, J. P.; Staroverov, V. N.; Scuseria, G. E. Climbing the Density Functional Ladder: Nonempirical Meta-Generalized Gradient Approximation Designed for Molecules and Solids. *Phys. Rev. Lett.* **2003**, *91*, 146401.
- (80) Peverati, R.; Truhlar, D. G. An improved and broadly accurate local approximation to the exchange–correlation density functional: The MN12-L functional for electronic structure calculations in chemistry and physics. *Phys. Chem. Chem. Phys.* **2012**, *14*, 13171–13174.
- (81) Mardirossian, N.; Ruiz Pestana, L.; Womack, J. C.; Skylaris, C.-K.; Head-Gordon, T.; Head-Gordon, M. Use of the rVV10 Nonlocal Correlation Functional in the B97M-V Density Functional: Defining B97M-rV and Related Functionals. *J. Phys. Chem. Lett.* **2017**, *8*, 35–40.
- (82) Perdew, J. P.; Ernzerhof, M.; Burke, K. Rationale for mixing exact exchange with density functional approximations. *J. Chem. Phys.* **1996**, *105*, 9982–9985.
- (83) Adamo, C.; Barone, V. Toward reliable density functional methods without adjustable parameters: The PBE0 model. *J. Chem. Phys.* **1999**, *110*, 6158–6170.
- (84) Becke, A. D. A new mixing of Hartree–Fock and local density-functional theories. *J. Chem. Phys.* **1993**, *98*, 1372–1377.
- (85) Rohrdanz, M. A.; Herbert, J. M. Simultaneous benchmarking of ground- and excited-state properties with long-range-corrected density functional theory. *The Journal of Chemical Physics* **2008**, *129*, 034107.
- (86) Rohrdanz, M. A.; Martins, K. M.; Herbert, J. M. A long-range-corrected density functional that performs well for both ground-state properties and time-dependent density functional theory excitation energies, including charge-transfer excited states. *The Journal of Chemical Physics* **2009**, *130*, 054112.
- (87) Yanai, T.; Tew, D. P.; Handy, N. C. A new hybrid exchange–correlation functional using the Coulomb-attenuating method (CAM-B3LYP). *Chem. Phys. Lett.* **2004**, *393*, 51–57.
- (88) Cohen, A. J.; Mori-Sánchez, P.; Yang, W. Development of exchange-correlation functionals with minimal many-electron self-interaction error. *The Journal of Chemical Physics* **2007**, *126*, 191109.
- (89) Krukau, A. V.; Vydrov, O. A.; Izmaylov, A. F.; Scuseria, G. E. Influence of the exchange screening parameter on the performance of screened hybrid functionals. *The Journal of Chemical Physics* **2006**, *125*, 224106.
- (90) Henderson, T. M.; Janesko, B. G.; Scuseria, G. E. Generalized gradient approximation model exchange holes for range-separated hybrids. *The Journal of Chemical Physics* **2008**, *128*, 194105.
- (91) Chai, J.-D.; Head-Gordon, M. Systematic optimization of long-range corrected hybrid density functionals. *J. Chem. Phys.* **2008**, *128*, 084106.
- (92) Chai, J.-D.; Head-Gordon, M. Long-range corrected hybrid density functionals with damped atom–atom dispersion corrections. *Phys. Chem. Chem. Phys.* **2008**, *10*, 6615–6620.
- (93) Lin, Y.-S.; Li, G.-D.; Mao, S.-P.; Chai, J.-D. Long-Range Corrected Hybrid Density Functionals with Improved Dispersion Corrections. *J. Chem. Theory Comput.* **2013**, *9*, 263–272.
- (94) Mardirossian, N.; Head-Gordon, M.  $\omega$ B97X-V: A 10-parameter, range-separated hybrid, generalized gradient approxima-

tion density functional with nonlocal correlation, designed by a survival-of-the-fittest strategy. *Phys. Chem. Chem. Phys.* **2014**, *16*, 9904–9924.

(95) Zhao, Y.; Truhlar, D. G. The M06 suite of density functionals for main group thermochemistry, thermochemical kinetics, non-covalent interactions, excited states, and transition elements: two new functionals and systematic testing of four M06-class functionals and 12 other functionals. *Theor. Chem. Acc.* **2008**, *120*, 215–241.

(96) Zhao, Y.; Truhlar, D. G. Exploring the Limit of Accuracy of the Global Hybrid Meta Density Functional for Main-Group Thermochemistry, Kinetics, and Noncovalent Interactions. *J. Chem. Theory Comput.* **2008**, *4*, 1849–1868.

(97) Yu, H. S.; He, X.; Li, S. L.; Truhlar, D. G. MN15: A Kohn–Sham global-hybrid exchange–correlation density functional with broad accuracy for multi-reference and single-reference systems and noncovalent interactions. *Chemical Science* **2016**, *7*, 5032–5051.

(98) Boese, A. D.; Martin, J. M. L. Development of density functionals for thermochemical kinetics. *J. Chem. Phys.* **2004**, *121*, 3405–3416.

(99) Staroverov, V. N.; Scuseria, G. E.; Tao, J.; Perdew, J. P. Comparative assessment of a new nonempirical density functional: Molecules and hydrogen-bonded complexes. *J. Chem. Phys.* **2003**, *119*, 12129–12137.

(100) Hui, K.; Chai, J.-D. SCAN-based hybrid and double-hybrid density functionals from models without fitted parameters. *J. Chem. Phys.* **2016**, *144*, 044114.

(101) Zhao, Y.; Truhlar, D. G. Hybrid meta density functional theory methods for thermochemistry, thermochemical kinetics, and noncovalent interactions: the MPW1B95 and MPWB1K models and comparative assessments for hydrogen bonding and van der Waals interactions. *J. Phys. Chem. A* **2004**, *108*, 6908–6918.

(102) Wang, Y.; Verma, P.; Zhang, L.; Li, Y.; Liu, Z.; Truhlar, D. G.; He, X. M06-SX screened-exchange density functional for chemistry and solid-state physics. *Proceedings of the National Academy of Sciences* **2020**, *117*, 2294–2301.

(103) Peverati, R.; Truhlar, D. G. Improving the Accuracy of Hybrid Meta-GGA Density Functionals by Range Separation. *J. Phys. Chem. Lett.* **2011**, *2*, 2810–2817.

(104) Verma, P.; Wang, Y.; Ghosh, S.; He, X.; Truhlar, D. G. Revised M11 Exchange-Correlation Functional for Electronic Excitation Energies and Ground-State Properties. *The Journal of Physical Chemistry A* **2019**, *123*, 2966–2990.

(105) Mardirossian, N.; Head-Gordon, M.  $\omega$  B97M-V: A combinatorially optimized, range-separated hybrid, meta-GGA density functional with VV10 nonlocal correlation. *J. Chem. Phys.* **2016**, *144*, 214110.

(106) Mardirossian, N.; Head-Gordon, M. Thirty years of density functional theory in computational chemistry: an overview and extensive assessment of 200 density functionals. *Mol. Phys.* **2017**, *115*, 2315–2372.

(107) Caldeweyher, E.; Ehlert, S.; Hansen, A.; Neugebauer, H.; Spicher, S.; Bannwarth, C.; Grimme, S. A generally applicable atomic-charge dependent London dispersion correction. *J. Chem. Phys.* **2019**, *150*, 154122.

(108) Epifanovsky, E.; Gilbert, A. T.; Feng, X.; Lee, J.; Mao, Y.; Mardirossian, N.; Pokhilko, P.; White, A. F.; Coons, M. P.; Dempwolff, A. L.; et al. Software for the frontiers of quantum chemistry: An overview of developments in the Q-Chem 5 package. *J. Chem. Phys.* **2021**, *155*, 084801.

(109) Dasgupta, S.; Herbert, J. M. Standard grids for high-precision integration of modern density functionals: SG-2 and SG-3. *Journal of computational chemistry* **2017**, *38*, 869–882.

(110) Rappoport, D.; Furche, F. Property-optimized Gaussian basis sets for molecular response calculations. *J. Chem. Phys.* **2010**, *133*, 134105.

(111) Martin, J. M.; de Oliveira, G. Towards standard methods for benchmark quality ab initio thermochemistry—W1 and W2 theory. *J. Chem. Phys.* **1999**, *111*, 1843–1856.

(112) Parthiban, S.; Martin, J. M. Assessment of W1 and W2 theories for the computation of electron affinities, ionization potentials, heats of formation, and proton affinities. *J. Chem. Phys.* **2001**, *114*, 6014–6029.

(113) Neese, F.; Valeev, E. F. Revisiting the atomic natural orbital approach for basis sets: Robust systematic basis sets for explicitly correlated and conventional correlated ab initio methods? *J. Chem. Theory Comput.* **2011**, *7*, 33–43.

(114) Helgaker, T.; Jorgensen, P.; Olsen, J. *Molecular electronic-structure theory*; John Wiley & Sons, 2014.

(115) Jin, Y.; Shi, Y.; Qi, X.; Huang, S.; Zhang, Q. Theoretical Study on Hydrolytic Stability of Borohydride-Rich Hypergolic Ionic Liquids. *J. Phys. Chem. A* **2020**, *124*, 2942–2950.

(116) Xie, X.; Clark Spotte-Smith, E. W.; Wen, M.; Patel, H. D.; Blau, S. M.; Persson, K. A. Data-Driven Prediction of Formation Mechanisms of Lithium Ethylene Monocarbonate with an Automated Reaction Network. *J. Am. Chem. Soc.* **2021**, *143*, 13245–13258.

(117) Muniz Filho, R. C. D.; Sousa, S. A. A. d.; Pereira, F. d. S.; Ferreira, M. M. C. Theoretical study of acid-catalyzed hydrolysis of epoxides. *J. Phys. Chem. A* **2010**, *114*, 5187–5194.

(118) Sundararajan, M.; Rajaraman, G.; Jayapal, P.; Tamilmani, V.; Venuvanalingam, P. An ab initio and DFT study on the hydrolysis of carbonyl dichloride. *J. Mol. Struct.* **2005**, *730*, 155–160.

(119) Becke, A. D. Density-functional thermochemistry. V. Systematic optimization of exchange-correlation functionals. *J. Chem. Phys.* **1997**, *107*, 8554–8560.

(120) Zhao, Y.; Truhlar, D. G. Density Functional for Spectroscopy: No Long-Range Self-Interaction Error, Good Performance for Rydberg and Charge-Transfer States, and Better Performance on Average than B3LYP for Ground States. *J. Phys. Chem. A* **2006**, *110*, 13126–13130.